*lubricants*

MDPI

*Article*

# Research on Wear of Micro-Textured Tools in Turning GH4169 during Spray Cooling

**Jingshu Hu, Jiaxuan Wei, Xinmin Feng * and Zhiwei Liu**

Key Laboratory of Advanced Manufacturing Intelligent Technology, Ministry of Education, Harbin University of Science and Technology, Harbin 150080, China; hujingshu@hrbust.edu.cn (J.H.); 2120110105@stu.hrbust.edu.cn (J.W.); lzw1361894040@163.com (Z.L.)

* Correspondence: fxmin7301@hrbust.edu.cn; Tel.: +86-13633640821

**Abstract:** In this study, the wear resistance of micro-textured tools was explored. Micro-textured tools with different morphologies were used in turning GH4169 during spray cooling. The tool wear on the rake face of the different micro-texture morphologies was investigated through simulation and experiments. Firstly, based on the existing research on bionics, micro-textures with five different morphologies were designed on the rake face of carbide tools. A simulation model of cutting GH4169 during spray cooling was established, and the tools with designed micro-textures were used in it. The influence of the different micro-texture morphologies on the tool wear was analyzed. Secondly, the designed micro-textured tools with five different morphologies were produced using a femtosecond laser. Cutting experiments were conducted using the micro-textured tools during spray cooling. The wear area of the rake face was measured based on the infinitesimal method, and the optimal morphology with the best anti-wear ability was obtained. This study provides technical support for the design and development of micro-textured tools with an improved cutting performance, and contribute to the promotion and application of micro-textured tools.

**Keywords:** micro-texture morphology; GH4169; tool wear; spray cooling



**Citation:** Hu, J.; Wei, J.; Feng, X.; Liu, Z. Research on Wear of Micro-Textured Tools in Turning GH4169 during Spray Cooling. *Lubricants* **2023**, *11*, 439. https://doi.org/10.3390/lubricants11100439

Received: 6 September 2023
Revised: 27 September 2023
Accepted: 28 September 2023
Published: 12 October 2023



## 1. Introduction

Nickel-based superalloy GH4169 is a kind of alloy that features high hardness, high strength, and excellent corrosion resistance and heat resistance, and can maintain good mechanical stability even in very harsh environments [1]. Because of its excellent performance, it has been widely used in the aerospace, automotive, and nuke industries, as well as in petrochemical and many other frontiers, in recent years. It is because of the above material properties that GH4169 is a difficult-to-process material. In the processing of GH4169, serious wear occurs in ordinary tools, which brings about a short lifespan and fast failure. How to improve the cutting performance of GH4169 and reduce tool wear is a key problem to be solved in the processing of GH4169 [2].

There are many reasons for tool wear in the cutting process, and some scholars have conducted relevant research on the influence of the cutting parameters and cooling and lubrication conditions on tool wear. Wu et al. carried out a superalloy turning test using a PCBN tool under high pressure cooling, and analyzed the tool wear under different cutting speeds and cooling pressures. The experimental results showed that with the increase in the cutting speed, the degree of tool wear first increases, then decreases, and subsequently increases, and the influence of the cooling pressure on tool wear is that the wear first decreases and then increases [3]. Liu et al. conducted cutting experiments on AISI 304 stainless steel using cemented carbide tools in minimum quantity cooling lubrication (MQCL) conditions, and studied the influence of the cutting parameters on tool wear under minimum quantity cooling lubrication. The experimental results show that the cutting speed has the greatest impact on tool wear, followed by the feed rate and cutting depth. At the same time, MQCL achieves a better surface quality and lower tool wear than MQL and

dry cutting [4]. Sharma et al. studied the effect of turning a Ti6Al-4V alloy with soybean oil in minimum quantity lubrication (MQL). The performance of the turning operation in dry and MQL environments was compared. The research results show that, compared with dry cutting, the tool wear rate is lower in the MQL cutting environment [5]. M. Ukamanal et al. studied the machinability of AISI 316 stainless steel turning in a dry cutting and spring impingement cooling environment through turning experiments. The test results show that, compared with dry machining, the processing under spray cooling technology produces a better surface finish, lower tool wear, and lower cutting temperature, making SIC an effective cooling technology in turning operations [6]. Zhang et al. carried out tool wear tests for the high-speed milling of 300 M steel under dry and cooling minimum quantity lubrication (CMQL) conditions. The experimental results show that, compared to dry cutting, CMQL technology can effectively reduce abrasive wear of the blade, bond wear on the blade surface, oxidative wear at the flank boundary, and mild diffusion wear [7].

In recent years, micro-textured tools based on the bionics theory have provided a new direction for tool wear reduction design and for the efficient cutting of difficult-to-machine materials such as superalloys [8,9]. A micro-textured tool is a tool in which micro-structures—such as convex, bulge, pit, groove, scale, and so on—are machined on its rake/flank face [10,11]. These micro-textured tools are more conducive to the penetration, storage, and film formation of lubrication medium, achieve a better friction reduction effect, slow down tool wear, and extend the service life of tools [12]. The high-performance-surface texture enables good friction reduction, adhesion resistance, and improved wear resistance. Cao Tongkun et al. used micro-textured tools to cut AISI 1045 steel and studied the friction coefficient, tool–chip contact length, and tool wear. The test results indicate that, in comparison to traditional pan-lubricated cutting, micro-textured tools provide a better cutting performance than other tools [13]. Using finite element analysis, Liu Wei et al. designed three different micro-textures on the rake face of cemented carbide tools—namely, a semicircular concave micro-texture, semicircular convex micro-texture, and trapezoidal groove micro-textured—and studied the influence of the micro-textured tools on the friction by changing the diameter or width of the micro-textures, the spacing of the micro-textures, and the covering length of the micro-textures. By analyzing the simulation data, we can see that, for the three tested micro-textured tools, the friction in cutting can be reduced by 23.0%, 27.7%, and 21.9%, respectively, using the optimal micro-texture parameters. In the range of the tool–chip contact length, the longer the micro-textured covering length, the better the anti-wear ability [14]. Yang G. et al. carried out internal-cooling-texture treatment on TNMG160404-SG XL7020 cemented carbide inserts using electric spark and laser technology, so that the rake face and the main flank face were internally cooled. Compared with non-woven tools, woven tools can reduce the tool–chip contact area, improve the anti-friction performance, and reduce the average friction coefficient of the interface between the tool and chip by about 2–8.6% [15]. Wu Ze et al. used elliptical micro-textured self-lubricating carbide tools and traditional tools to carry out a comparative test of dry cutting 45 steel. Compared with traditional tools, micro-textured self-lubricating tools can effectively reduce the rake face wear [16]. Huang Ke et al. used a nanosecond laser to process grooves on the tool surface, and designed dry friction and wear tests for micro-textured tools with different area occupancy rates. The experimental results indicate that the micro-textured tools can store the debris generated by friction, reduce the roughness of the tool surface, and fully reflect the influence of the micro-texture on the anti-wear ability [17]. Long Yuanqiang et al. used a micro-textured self-lubricating tool, micro-textured tool, and traditional carbide tool to carry out dry cutting tests on 0Cr18Ni9 austenitic stainless steel. Through analyzing the experimental data, it was concluded that micro-textured self-lubricating tools can effectively improve the adhesive wear of tools [18]. Li Liang et al. studied the anti-wear ability of the surface micro-textured tool under the condition of minimal lubrication and no lubricant through an orthogonal cutting experiment of titanium alloy. Based on the experimental data, it can be concluded that surface micro-grooves can effectively improve the friction of the tool chips

under the condition of lubricant in order to achieve an improved anti-wear ability [19]. In order to verify the anti-wear ability of micro-textured tools, Tu Chunjuan used micro-pit and micro-groove texture self-lubricating tools to turn hardened steel. The experimental results show that the micro-pit-textured tools show a better wear reduction performance than the micro-groove-textured tools [20].

Some research results have also been obtained on the influence of different micro-textured arrangements on the wear: Arulkirubakaran D et al. conducted numerical simulation and turning experiments on a Ti-6Al-4V alloy using surface-textured tungsten carbide tools. The tool has micro-grooves parallel, perpendicular, and intersecting with the direction of chip flow. The numerical simulation results were validated by the experimental results, which include the cutting temperature, machining force, and chip morphologies. Cutting tools with surface textures processed in a direction perpendicular to that of the chip flow exhibited a larger reduction in the cutting force, temperature generation, and reduced tool wear [21]. Tatsuya Sugihara developed a CBN micro-textured tool with a micro-groove on the flank face, and the groove micro-textured arrangement was perpendicular to the cutting edge; the cutting test was carried out on Inconel 718. The results indicate that the micro-textured tool significantly extends the service life of CBN tools for high-speed dry cutting Inconel 718 [22]. Fang Zhenglong et al. produced five different shapes of micro-textures on the flank face, and the arrangement of the micro-textures was mainly parallel or vertical to the cutting edges. The wear of a micro-textured tool and a non-textured tool in the longitudinal turning process of an Inconel 718 nickel-based superalloy was compared in the condition of high-pressure jet assisted cooling. It was seen that, in comparison to non-textured tools, tools with micro-textures have lower flank face wear and crescent wear, and the arrangement of the micro-textures will affect the tool wear rate. In particular, tools with micro-textures of plate-fins showed a better performance than those with pin-fins [23]. Based on the energy loss method, Zhang Yan et al. established the micro-textured tool continuous wear model in the process of micro-cutting Ti6Al4V titanium alloy material using a carbide tool in ABAQUS6.14-5, and designed single and multiple micro-texture models at different positions of the rake face to analyze the influence of the micro-textures on the rake face depression wear and the flank face wear. The analysis shows that the quantity and position of the micro-textures on the rake face have a marked impact on the wear of tools with no texture [24]. Duan et al. carried out cutting experiments on Inconel 718 using three kinds of micro-textured CBN tools; namely, pit, straight line, and sine. The cutting force, tool wear, and machined surface roughness of the different micro-textured tools were compared and analyzed. The experimental results show that the existence of surface micro-texture enhances the wettability of the tool surface. It effectively reduces the cutting force, the wear of the rake face, and the surface roughness of the machined parts. Compared with other morphologies, the sinusoidal micro-textured tool shows the best cutting performance [25].

Based on the above studies, it can be seen that micro-textures have a significant effect on the improvement of the cutting performance of tools, especially in the reduction in tool wear. The existing studies of materials for workpiece cutting using micro-textured tools mainly focus on titanium alloy, aluminum alloy, stainless steel, hardened steel, and other difficult-to-cut materials. However, few studies have been conducted on the tool wear of micro-textured tools used to cut GH4169, and there are even fewer studies on the properties of micro-textured tools during spray cooling. In this article, experiments of turning a nickel-based GH4169 superalloy using micro-textured tools during spray cooling were carried out to investigate the influence of different micro-texture morphologies on the wear of tools. This study aims to provide technical reference for the design and application of micro-textured tools.

## 2. Design and Processing of Micro-Textured Tools

### *2.1. Distribution of Micro-Textures*

The distribution of micro-textures takes two factors into account: the tool–chip contact length and the wear area of the rake face. Based on a series of cutting experiments and simulation studies, it was found that the maximum tool–chip contact length of the cemented carbide tool in turning GH4169 was about 500–700 μm from the nose of the tool, and the wear area on the rake face was within 500 μm of the tool nose [26].

### *2.2. Morphology of Micro-Textures*

Studies have shown that the micro-texture morphology has an important impact on its anti-wearability. A micro-texture with an unreasonable shape and size not only fails to achieve the purpose of wear reduction, but will aggravate the wear of the tool and reduce the strength of the tool [27].

Based on the research of bionics, the surface characteristics of natural creatures were observed under microscope and studied in terms of anti-friction performance. The body surface structure of the creatures is shown in Figure 1.

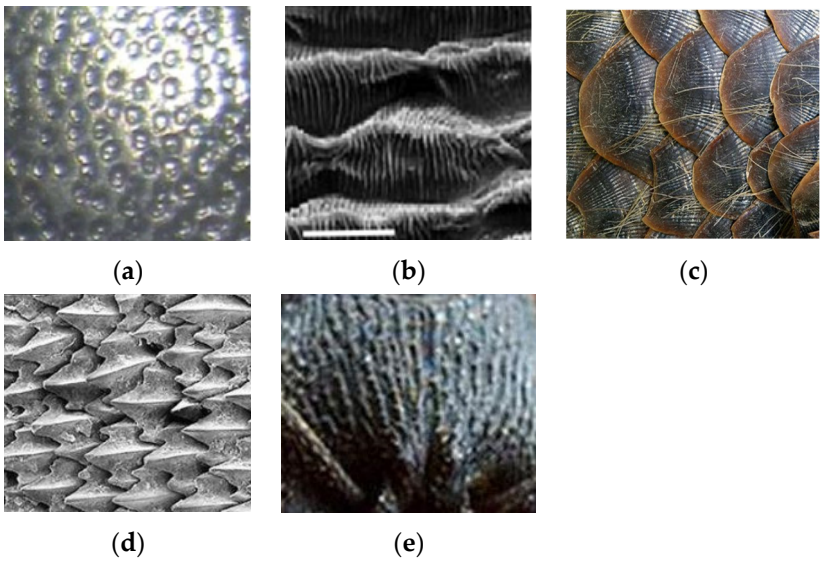


**Figure 1.** Body surface structure of creatures: (**a**) pit-structure on dung beetle shells; (**b**) waveform grooves on the shells of scapharca broughtonii; (**c**) straight and curved grooves on the shells of pangolin scales; (**d**) arrowtooth-shaped textures on shark skin; (**e**) straight grooves on the shells of ant.

In this work, five micro-texture morphologies were designed according to the study on the surface characteristics of natural creatures; namely, micro-pit, micro-wave-groove, micro-arc-groove, micro-vertical-groove, and micro-elliptic-groove. The schematic diagram of the micro-texture morphologies is shown in Figure 2.

The femtosecond laser method was used to process the micro-textures of different morphologies on the rake face of the cemented carbide tool, as shown in Figure 3. The distance of the micro-texture from the tool tip was 120 μm and the depths processed in this work were all 30 μm.

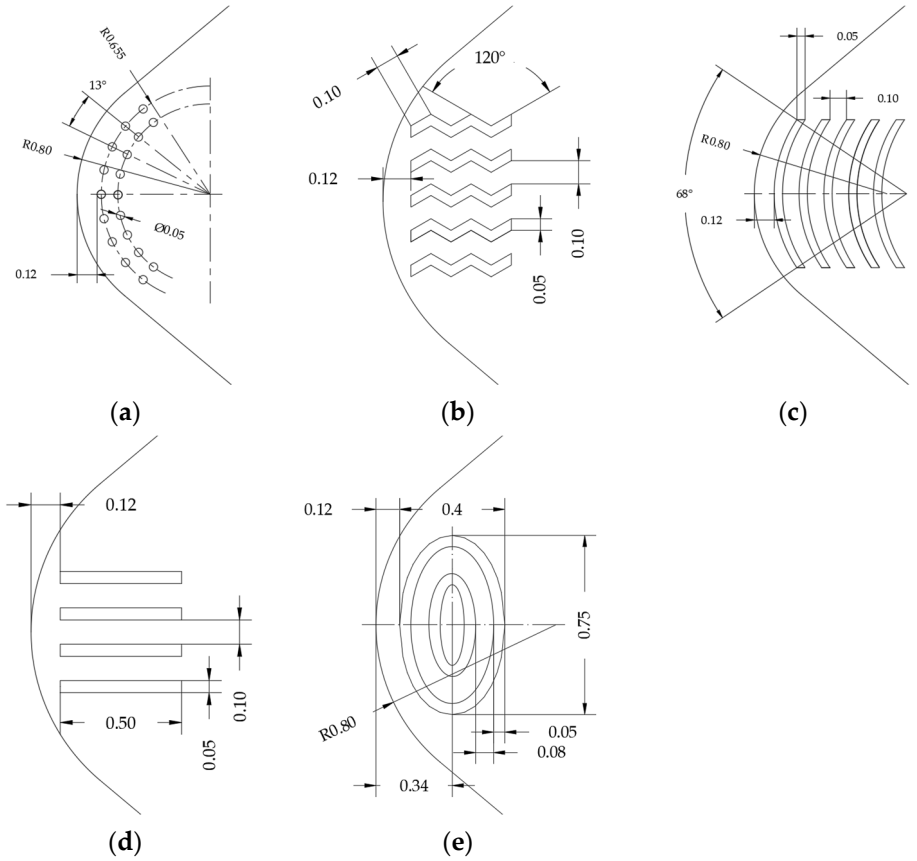


**Figure 2.** Schematic diagram of micro-texture morphologies: (**a**) micro-pit; (**b**) micro-wave-groove; (**c**) micro-arc-groove; (**d**) micro-vertical-groove; (**e**) micro-elliptic-groove.

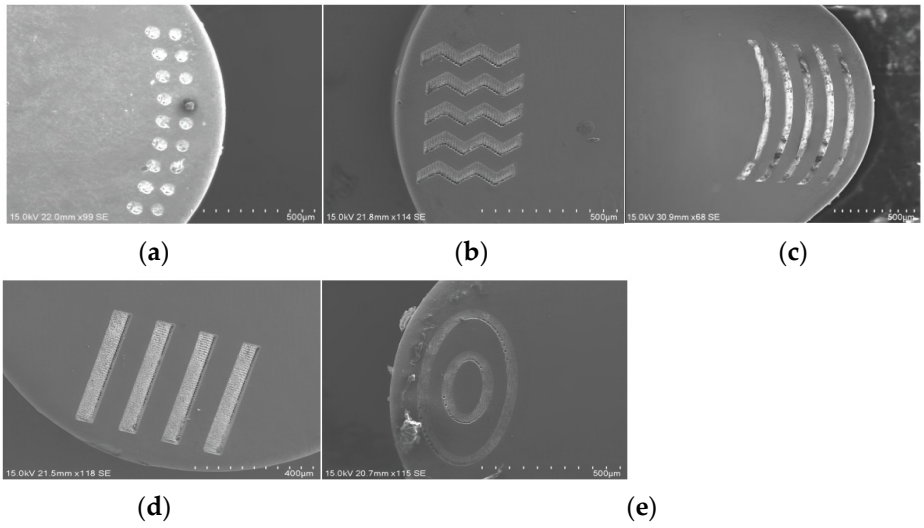


**Figure 3.** Partial larger views of the nose of the micro-textured tools: (**a**) micro-pit; (**b**) micro-wave-groove; (**c**) micro-arc-groove; (**d**) micro-vertical-groove; (**e**) micro-elliptic-groove.

## 3. Tool Wear Simulation Analysis

### *3.1. Establishment of Cutting Simulation Model*

(1) Construction of tool geometric model

The geometric models of the micro-textured tools with five different morphologies, established in the proportion of 1:1, are shown in Figure 4.

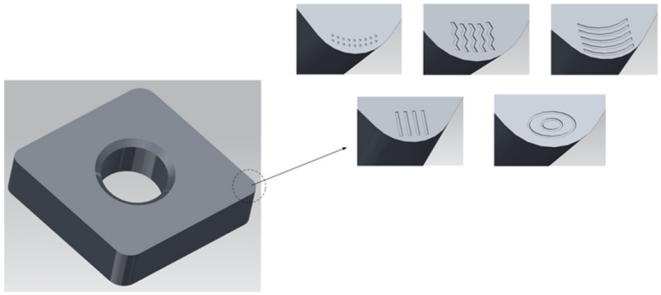

**Figure 4.** Geometric model and enlarged drawing of micro-textured tool.

The rake face used in this study was designed with micro-textures, which need to be refined in the mesh. In order to conduct simulation analysis efficiently, the cylindrical workpiece is selected as part of the thin-walled ring rotary workpiece, and the tool is simplified into the tool nose part. The simplified cutting model is shown in Figure 5.

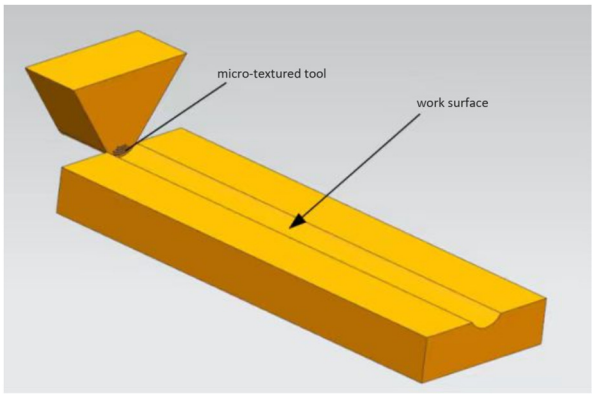


**Figure 5.** Simplified cutting model.

(2) Workpiece material model

The Johnson–Cook constitutive model considers the strain hardening, strengthening, and thermalization of the material, which are closer to the actual phenomenon. The Deform software (Deform 11.0) comes with a rich material library. The simulation workpiece material is a nickel-based superalloy. In this simulation, the existing Inconel718 (performance similar to GH4169) in the Deform material library was selected, and the mathematical expression of the Johnson–Cook constitutive model was selected for the constitutive model. The material model expression is shown in Equations (1) and (2):

$$\overline{\sigma} = \overline{\sigma}(\overline{\varepsilon}, \dot{\overline{\varepsilon}}, T) = (A + B\overline{\varepsilon}^{n})(1 + C\ln\dot{\overline{\varepsilon}})(1 - T^{*m}) \quad (1)$$

$$T^{*} = \frac{T - T_{room}}{T_{melt} - T_{room}} \quad (2)$$

where $\overline{\sigma}$ is the flow stress; $\overline{\sigma}$ is the equivalent plastic strain; $\dot{\overline{\varepsilon}}$ is the equivalent plastic strain rate; T is the deformation temperature; A is the yield stress; B is the pre-exponential coefficient; C is the strain rate sensitivity coefficient; m is the temperature sensitivity coefficient; n is the hardening coefficient; $T^{*}$ is the relative temperature; $T_{melt}$ and $T_{room}$ are the melting temperature and room temperature of the workpiece material, respectively.

The J–C constitutive model parameters of the workpiece material are shown in Table 1.

**Table 1.** Johnson–Cook constitutive model parameters of Inconel 718.

| ρ/(kg/m$^3$) | $C_P$/J·kg$^{-1}$·K$^{-1}$ | E/GPa | A/MPa | B/MPa |
|---|---|---|---|---|
| 8240 | 435 | 200 | 450 | 1700 |
| **C** | **m** | **n** | $\dot{\varepsilon}$/s$^{-1}$ | $T_{melt}$/°C |
| 0.017 | 1.3 | 0.65 | 0.001 | 1300 |

(3) Tool–chip friction model

Because the simulation is the process of cutting the nickel-based superalloy using a micro-textured tool, the tool nose is heated faster in the rake face during cutting, and the temperature difference between the tool nose and the rake face is generated, which reduces the normal stress ratio, and sliding friction occurs between the two cutting tools. In order to ensure the accuracy of the simulation and to accurately select the type of friction, the mixed-slip friction model was chosen in this simulation. The model expression is shown in Equation (3):

$$\begin{cases} T_f = \mu\sigma_n (\text{Sliding zone}, \mu\sigma_n \le \tau_n) \\ T_f = \tau_n (\text{Bonding zone}, \mu\sigma_n \ge \tau_n) \end{cases} \quad (3)$$

where $T_f$ is the friction stress; $\sigma_n$ is the normal stress; $\mu$ is the friction coefficient, this simulation takes $\mu$ as 0.6; $\tau_n$ is the ultimate shear stress of the workpiece.

(4) Mesh division and wear calculation model

When the tool model is divided into meshes, the micro-textured part needs to be locally refined. The mesh division method is absolute mesh division, the total number of meshes is 55,000, the minimum mesh size is 0.015 mm, and the mesh refinement ratio is 6. Taking the micro-arc-groove as an example, the divided mesh model is shown in Figure 6.

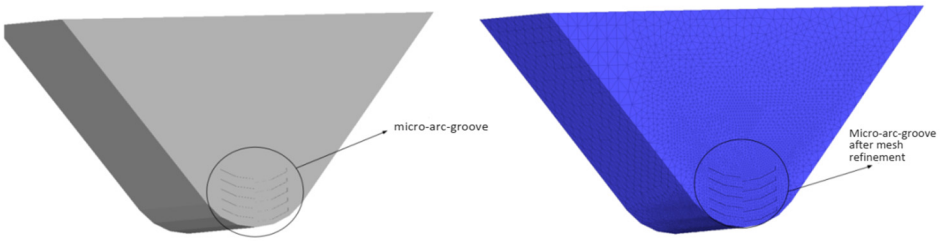


**Figure 6.** Grid division of micro-textured tool with arc groove.

As the simulation mainly observes the wear of the tool, the wear model needs to be selected during the setting. In Deform-3D preprocessing, there is a Usui wear model, and users can also set the wear model according to their own needs. In order to fit the actual cutting conditions and meet the existence of harsh conditions, such as a high strain rate, high temperature, and high pressure, the Usui calculation model is selected. Its mathematical expression is shown in Equation (4).

$$w = \int apVe^{-\frac{b}{T}} dt \quad (4)$$

where w is the wear depth; p is the chip interface stress; V is the slip velocity; T is the interface temperature; dt is the time increment; a and b are constants, according to the material properties of the tool, a is set to $1 \times 10^{-6}$ and b is set to 855.

### *3.2. Simulation of Spray Cooling*

As the simulation conducts a cutting test in the cutting environment of spray cooling, there is no direct setting of the spray cooling parameter conditions in the Deform software preprocessing; therefore, the research group uses the ANSYS simulation software (ANSYS

16.0) to simulate spray cooling, and analyzes the influence of different spray flow rates and pressures on the cutting temperature and convective heat transfer coefficient through the simulation and test. By means of the range analysis method, the optimal combination of spray parameters is obtained, with the lowest cutting temperature as the target. When the spray pressure is 0.3 Mpa and the flow rate 3.16 L/h, the corresponding convective heat transfer coefficient is 3.13737 w/m$^2$-k [28]. The convective heat transfer coefficient under the optimal parameters is imported into the Deform software, which can be equivalent to cutting under the condition of spray cooling.

In order to ensure the comparability of the simulation results and to reduce the influence of other condition settings on the simulation results, the analysis step size was set to 1500, step size increment to 0.01, ambient temperature to 20 °C, and friction factor to 0.6 for the five designed micro-textured tools.

### *3.3. Analysis of Simulation Results*

A simulation of cutting GH4169 using the micro-textured tools was conducted with the same cutting parameters: the cutting speed V was set to 80 m/min; the feed rate was 0.2 mm/r; and the depth of cut $a_p$ 0.2 mm. The finite element analysis of the tool wear obtained after cutting is shown in Figure 7.

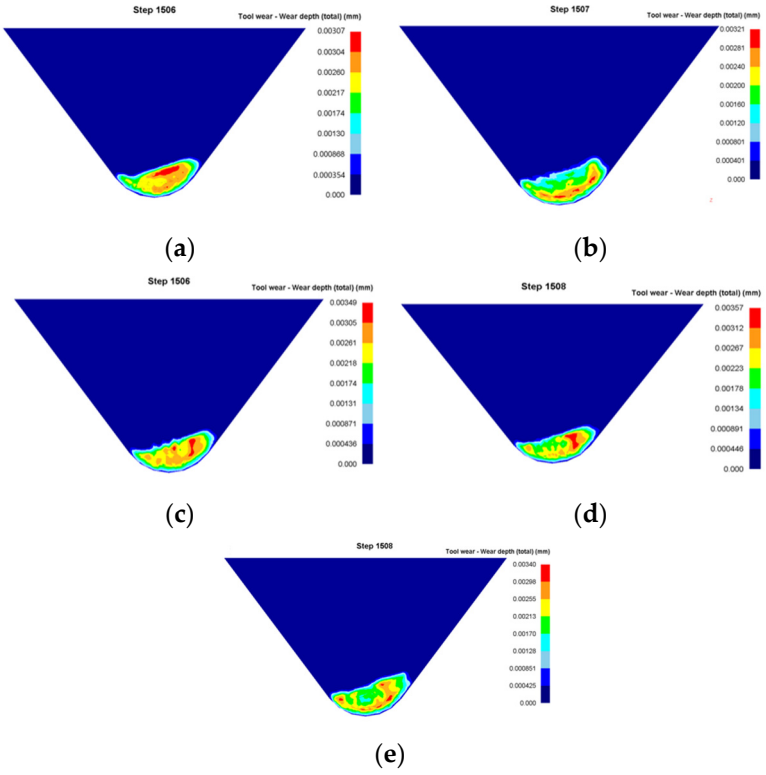


**Figure 7.** Finite element analysis of tool wear: (**a**) micro-pit; (**b**) micro-arc-groove; (**c**) micro-vertical-groove; (**d**) micro-wave-groove; (**e**) micro-elliptic-groove.

By observing Figure 7, it is found that deep wear bands appear on the rake face of the five kinds of micro-textured tools near the arc of the tool nose. In order to explore the changing trend of the wear depth of the five kinds of micro-textured tools with different morphologies, at the wear band near the radius of the arc of the tool nose, the same coordinate point is taken as the unit of 200 simulation step lengths and the simulation step length is changed. The tool wear depth of the five kinds of micro-textures is shown in Figure 8.

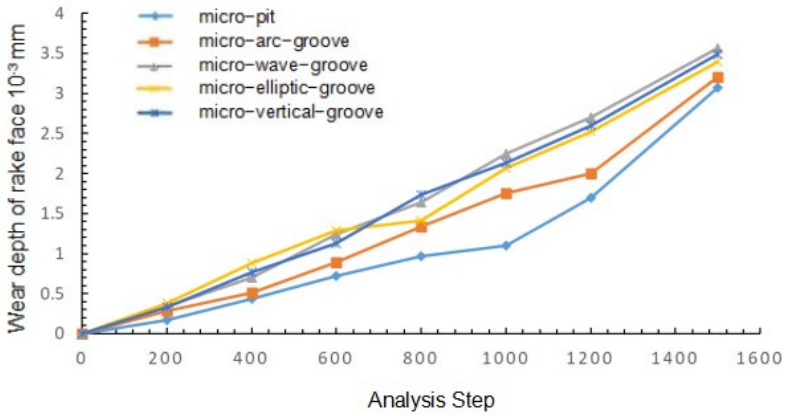


**Figure 8.** The wear depth of five kinds of micro-textured tools.

The wear depth of the rake face is shown in Table 2.

**Table 2.** The wear depth of rake face of micro-textured tools with different morphologies.

| Micro-Textured Morphology | Minimum Wear Depth of the Rake Face ($10^{-3}$ mm) | Maximum Wear Depth of the Rake Face ($10^{-3}$ mm) |
|---|---|---|
| micro-pit | 0.354 | 3.07 |
| micro-arc-groove | 0.401 | 3.21 |
| micro-vertical-groove | 0.436 | 3.49 |
| micro-wave-groove | 0.446 | 3.57 |
| micro-elliptic-groove | 0.425 | 3.4 |

It can be seen from Table 2 that under the same coordinates, the wear depth of the micro-pits' morphology changed the least with the simulation steps. By combining the cloud map of the wear changes of the five micro-textured tools, it can be found that the wear distribution of the micro-pit-textured tool on the rake face is more dispersed, and the wear depth value had the smallest variation range. Moreover, the maximum wear depth of the micro-pit-textured tools had a smaller distribution near the tool tip, and the maximum wear depth is more dispersed than the other tools. It can be seen that the micro-pit-textured tool had the smallest wear depth on the rake face, and its anti-wear capacity was better than the other micro-textured tools.

## 4. Cutting Experiment during Spray Cooling

### *4.1. Conditions of Experiment*

Micro-textured tools with different morphologies were used in a turning experiment during spray cooling. The workpiece size was Φ 120 × 300 mm; the tool shank was Sandvik DCLNR 2525 M12; the insert was CNMA120408-KR 3225; and the micro-texture was processed on the rake face, as shown in Figure 5. The adopted cooling equipment was produced by Anmolin using the OoW129S model and the working pressure was in the range of 0.3 MPa to 0.8 MPa. The angle between the spray nozzle and rake face was 45 degrees, and the spray nozzle was 20 mm away from the tool nose. The nozzle outlet pressure was 0.3 MPa, and the flow rate was 3 L/h; the main components of the cutting fluid are mixed with Master and Castrol. The cutting parameters were as follows: v was 80 m/min; f was 0.2 mm/r; $a_p$ was 0.2 mm; and cutting time was 30 s. The experiment setup is shown in Figure 9.


(**a**) (**b**)

**Figure 9.** Experiment setup: (**a**) spray cooling site; (**b**) spray cooling equipment.

*4.2. Analysis of Experiment Results*

The rake faces of the micro-textured tools with different morphologies were observed through scanning electron microscopy, as shown in Figure 10.

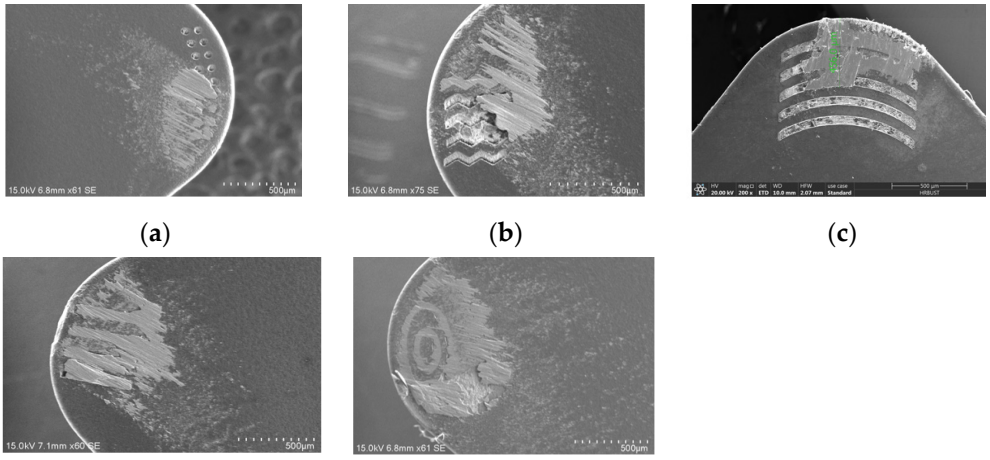

(**a**) (**b**) (**c**)

(**d**) (**e**)

**Figure 10.** Tool wear of the rake face with different morphologies: (**a**) micro-pit; (**b**) micro-wave-groove; (**c**) micro-arc-groove; (**d**) micro-vertical-groove; (**e**) micro-elliptic-groove.

As shown in Figure 11, the wear area of the rake face is an irregular geometric shape, which enables us to compare the wear degree of the rake face of each set of tools in the experiment. This experiment uses the rectangular equivalent area method, and the wear area calculated using the infinitesimal method is equivalent to a rectangular wear zone of equal area to indicate the degree of wear on the rake face.

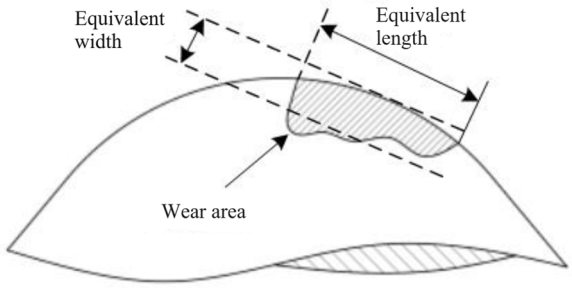


**Figure 11.** Wear area of the rake face.

In this experiment, the infinitesimal method is used to calculate the area of the wear area of the rake face. Divide the wear area into n small rectangles, the width of i is $l_i$, measuring the height of the rectangle separately; then, the whole area is:

$$S = l_1 \times h_1 + l_2 \times h_2 + \ldots + l_n \times h_n = \sum_{i=1}^{n} l_i \times h_i = w \times l \quad (5)$$

$$l = l_1 + l_2 + \ldots + l_n = \sum_{i=1}^{n} l_i \quad (6)$$

where S is the equivalent rectangular wear zone area; w is the equivalent width of the rectangular wear zone; and l is the equivalent rectangular wear zone length.

The calculation results of the wear area of the rake face of the five micro-textured tools using the infinitesimal method are shown in Table 3, and the histogram of the wear area of the rake face of the five micro-textured tools is shown in Figure 12.

**Table 3.** The wear area of rake face of five kinds of micro-textured tools.

| Micro-Textured Morphology | Equivalent Band Width w/μm | Equivalent Belt Length l/μm | Wear Area S/μm$^2$ |
|---|---|---|---|
| micro-pit | 37.8 | 337.1 | 12,762.5 |
| micro-elliptic-groove | 30.71 | 805.86 | 24,754.7 |
| micro-arc-groove | 23.4 | 659.3 | 15,395.6 |
| micro-wave-groove | 32.7 | 637.3 | 20,851.1 |
| micro-vertical-groove | 29.4 | 687.9 | 20,229.7 |

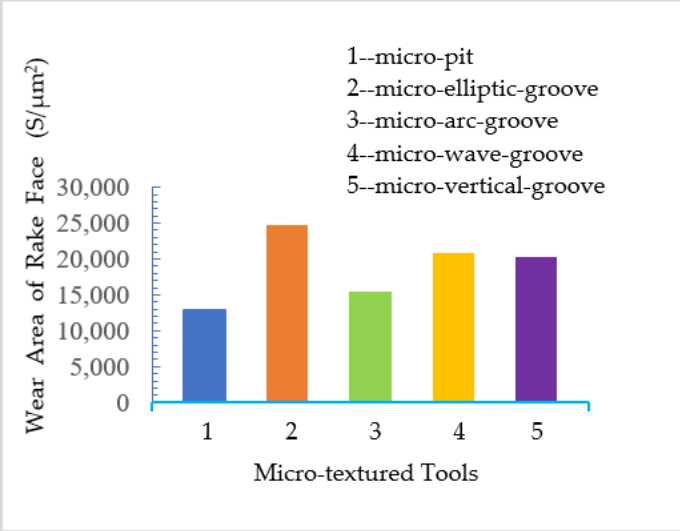


**Figure 12.** The wear area of rake face of micro-textured tools.

The experiment results showed that among the five designed micro-textured tools, the ones with micro-pits had the smallest wear area, and the wear area was relatively far away from the tool nose. The micro-textured tools with micro-pits achieved the best anti-wear ability. The experimental results verified the simulation results.

## 5. Conclusions

In this study, five micro-textured tools with different morphologies were used in cutting GH4169 during spray cooling. The research was conducted through both finite element simulations and experiments. The influence of micro-textures with different morphologies on the tool wear was revealed. The optimal morphology of the micro-texture was obtained. The conclusions are as follows:

(1) A cutting simulation model was established in a spray cooling condition. The effect of the micro-texture morphologies on the wear of the rake face was obtained. A series of

experiments were conducted with the same spray cooling parameters. The results of the experiments on the tool wear conformed to those of the simulation. The reliability of the simulation was verified.

(2) The insertion of micro-textures can effectively improve the anti-wear ability of micro-textured tools on the tool–chip interface and reduce tool wear. The distribution of the micro-textures was set within the working area; it measured a distance of 60–120 μm from the top micro-texture to the edge of the tool nose, and the other micro-textures were set in the area 500 μm away from the tool nose.

(3) The simulation and experiment results showed that the micro-pits had a significantly better anti-wear ability than the other four morphologies. The wear depth of the rake face ranged between $0.354 \times 10^{-3}$ and $3.07 \times 10^{-3}$ mm, and the wear area of the rake face was 12,762.5 $\mu m^2$.

This article reveals the influence of micro-textured tools with different morphologies on tool wear. The conclusion of the article was drawn from a series of experiments and simulations, and it provides technical reference for both the machining of GH4169 and the application of micro-textured tools. However, many factors also contribute to tool wear in cutting, such as the size parameters of the micro-textures, the geometric parameters of the tools, the cutting parameters, etc. These factors were not considered in this article; therefore, it is necessary to conduct further related research.

**Author Contributions:** Methodology, J.H.; software, J.W.; validation, Z.L.; writing—original draft preparation, J.H.; writing—review and editing, X.F. All authors have read and agreed to the published version of the manuscript.

**Funding:** This study was supported by the National Natural Science Foundation of China (No. 51675144).

**Data Availability Statement:** Not applicable.

**Conflicts of Interest:** The authors declare no conflict of interest.

## References

1. Zheng, J.J.; Guo, Y.; Liu, X.; Zhang, Z.H.; Zhang, T. Introduction on Research and Application of Nickel Base Superalloy GH4169. *IOP Conf. Ser. Earth Environ. Sci.* **2021**, *651*, 022081. [CrossRef]
2. Yu, W.W.; Ming, W.W.; An, Q.L.; Chen, M. Cutting performance and wear mechanism of honeycomb ceramic tools in interrupted cutting of nickel-based superalloys. *Ceram. Int.* **2021**, *47*, 18075–18083. [CrossRef]
3. Wu, M.Y.; Wu, S.J.; Chu, W.X.; Cheng, Y.N. Experimental Study on Tool Wear in Cutting Superalloy under High-Pressure Cooling. *Integr. Ferroelectr.* **2020**, *207*, 208–219. [CrossRef]
4. Liu, N.C.; Zheng, C.L.; Xiang, D.Y.; Huang, H.; Wang, J. Effect of cutting parameters on tool wear under minimum quantity cooling lubrication (MQCL) conditions. *Int. J. Adv. Manuf. Technol.* **2019**, *105*, 515–529. [CrossRef]
5. Sharma, S.; Das, P.P.; Ladakhi, T.Y.; Pradhan, B.B.; Phipon, R. Performance Evaluation and Parametric Optimization of Turning Operation of Ti6Al-4V Alloy Under Dry and Minimum Quantity Lubrication Cutting Environments. *J. Mater. Eng. Perform.* **2022**, *32*, 5353–5364. [CrossRef]
6. Ukamanal, M.; Mishra, P.C.; Sahoo, A.K. Effects of Spray Cooling Process Parameters on Machining Performance AISI 316 Steel: A Novel Experimental Technique. *Exp. Tech.* **2020**, *44*, 19–36. [CrossRef]
7. Zhang, H.P.; Wang, Z.J.; Liu, G.L. Tool Wear of High-speed Machining 300 M Steel Under CMQL Condition. *J. Harbin Univ. Sci. Technol.* **2020**, *25*, 75–82.
8. Ren, L.Q.; Han, Z.W.; Li, J.Q.; Tong, J. Experimental investigation of bionic rough curved soil cutting blade surface to reduce soil adhesion and friction. *Soil Tillage Res.* **2004**, *85*, 1–12. [CrossRef]
9. Zhang, N.; Yang, F.Z.; Liu, G.H. Cutting performance of micro-textured WC/Co tools in the dry cutting of Ti-6Al-4V alloy. *Int. J. Adv. Manuf. Technol.* **2020**, *107*, 3967–3979. [CrossRef]
10. Han, Z.L.; Wang, J.D.; Chen, D.R. Drag Reduction by Samples on Surfaces in Plane Contact Lubrication. *Tribology* **2009**, *29*, 10–16.
11. Han, Z.W.; Ren, L.Q.; Liu, Z.B. Investigation on Anti-wear Ability of Bionic Non-smooth Surfaces Made by Laser Texturing. *Tribology* **2004**, *4*, 289–293.
12. Kishawy, H.A.; Salem, A.; Hegab, H.; Hosseini, A.; Balazinski, M. Micro-textured cutting tools: Phenomenological analysis and design recommendations. *CIRP Ann.* **2021**, *70*, 65–68. [CrossRef]
13. Cao, T.K.; Li, Z.G.; Zhang, S.G.; Zhang, W.F. Cutting performance and lubrication mechanism of micro-texture tool with continuous lubrication on tool-chip interface. *Int. J. Adv. Manuf. Technol.* **2023**, *125*, 1815–1826. [CrossRef]

14. Liu, W.; Liu, S.; Liang, G.Q.; Yuan, H.C. Element analysis on cutting performance and friction reduction effect of micro-texture tools. *Surf. Technol.* **2022**, *51*, 338–346.
15. Yang, G.; Feng, W. Short communication: Experiment study on micro-textured tool with internal cooling. *Mech. Sci.* **2022**, *13*, 619–623. [CrossRef]
16. Wu, Z.; Deng, J.X.; Xin, Y.Q.; Cheng, J.; Zhao, J. Cutting performance of self-lubricating turning tools with elliptical micro-textures. *Trans. Chin. Soc. Agric. Mach.* **2012**, *43*, 228–234.
17. Huang, K.; Yang, F.Z.; Zheng, K.R.; Yi, B. Design and Manufacture of Micro Texture on Tool Surface and Its Influence on Friction Characteristics. *Tool Eng.* **2022**, *56*, 37–42.
18. Long, Y.Q.; Deng, J.X.; Zhou, H.M.; Zhao, W.; Wang, Z. Performance of Self-lubricating Micro-texture Tool on Dry Cutting 0Cr18Ni9 Austenitic Stainless Steel. *Mater. Mech. Eng.* **2015**, *39*, 75–79.
19. Qi, B.Y.; Li, L.; He, N.; Zhao, W.; Wang, Z. Experimental Study on Orthogonal Cutting of Ti6Al4V with Surface Micro-textured Cutting Tool. *Tribology* **2011**, *31*, 346–351. [CrossRef]
20. Tu, C.J.; Guo, X.H.; Guo, D.L.; Chen, Y.D.; Guan, J.J. Comparison of Machinability of Self-lubrication Ceramic Tools with Different Morphological Micro-textures. *Mater. Mech. Eng.* **2018**, *42*, 47–51, 57.
21. Arulkirubakaran, D.; Senthilkumar, V.; Kumawat, V. Effect of micro-textured tools on machining of Ti-6Al-4V alloy: An experimental and numerical approach. *Int. J. Refract. Met. Hard Mater.* **2016**, *54*, 165–177. [CrossRef]
22. Tatsuya, S.; Yuki, N.; Toshiyuki, E. Development of a novel cubic boron nitride cutting tool with a textured flank face for high-speed machining of Inconel 718. *Precis. Eng.* **2017**, *48*, 75–82.
23. Fang, Z.L.; Toshiyuki, O. Cooling performance of micro-texture at the tool flank face under high pressure jet coolant assistance. *Precis. Eng.* **2017**, *49*, 41–51. [CrossRef]
24. Zhang, Y.; Li, Q.H.; Yang, F.S. Simulation and Model of Micro-textured Tool Continuous Wear. *Tool Eng.* **2022**, *56*, 76–81.
25. Duan, Z.F.; Chen, L.; Li, B.B. Effect of micro-textured morphology with different wettabilities on tool cutting performance. *The Int. J. Adv. Manuf. Technol.* **2022**, *123*, 1745–1754. [CrossRef]
26. Yu, C. Research on Cutting Performance and Anti-wear Mechanism of Tools with Micro-texture under Spray Cooling. Master's Thesis, Harbin University of Science and Technology, Harbin, China, 2020.
27. Zhang, G.F.; Zhang, B.W. Influence of the micro-textured parametric variations on the cemented carbide fraction characteristics. *J. Mach. Des.* **2017**, *34*, 25–30.
28. Feng, X.M.; Dong, Q.S.; Hu, J.S.; Wang, B.H. Simulation and Experimental Analysis of Cutting Temperature in Cutting of Superalloy GH4169 under Spray. *Mech. Sci. Technol. Aerosp. Eng.* **2021**, *41*, 985–991.